# Covariance-Matrix-Based Vector-Network-Analyzer Uncertainty Analysis for Time- and Frequency-Domain Measurements*

Arkadiusz Lewandowski, *Member, IEEE,* Dylan F. Williams, *Fellow, IEEE,*
Paul D. Hale, *Senior Member, IEEE,* Jack C. M. Wang, and Andrew Dienstfrey

***Abstract*—We develop a covariance-matrix-based uncertainty analysis for vector-network-analyzer scattering-parameter measurements. The covariance matrix captures all of the measurement uncertainties and statistical correlations between them. This allows the uncertainties of vector-network-analyzer scattering-parameter measurements to be propagated into the uncertainties of other quantities derived from scattering parameters, including temporal waveforms.**

***Index Terms*—covariance matrix, vector network analyzer, scattering parameters, uncertainty analysis, frequency-domain measurements, time-domain measurements**

## I. Introduction

We develop a new uncertainty analysis for vector-network-analyzer (VNA) scattering-parameter (S-parameter) measurements. The key feature of our approach is that the VNA measurement uncertainties we provide can be translated into the uncertainty of any other quantity derived from the S-parameters. In particular, our uncertainties can be propagated into the time domain and used in the uncertainty analysis of time-domain measurement systems that involve frequency-domain VNA characterization. Such systems include electro-optic measurement systems [1], high-frequency sampling oscilloscopes [2, 3] and large-signal network analyzers [4].

Covariance-matrix descriptions of S-parameter measurement uncertainties have already been employed in some early contributions on six-port measurement systems. References [5, 6], for example, present a comprehensive covariance-matrix-based uncertainty analysis of a single-frequency S-parameters measurement in a 2-18 GHz dual six-port measurement system.

Recently, a covariance-matrix uncertainty description for S-parameter measurements was presented in [1, 7, 8]. References [7, 8] demonstrate that statistical correlations between measurement uncertainties for different S-parameters are required when propagating S-parameter measurement uncertainties into uncertainties of other frequency-domain quantities. References [7, 8] capture these correlations in covariance matrices of a form similar to the one suggested in [5]. Reference [1] generalizes those results and shows that in the case of propagation into temporal-domain quantities, statistical correlations between S-parameter measurement uncertainties for *different* frequencies become essential. Reference [1] captures these correlations in a multi-frequency covariance matrix, that is, a covariance matrix that accounts for the uncertainties and statistical correlations between them for all measurement frequencies. We use the representation introduced in [1] in this work.

Typical approaches to the VNA S-parameter measurement uncertainty analysis do not account for the statistical correlations between S-parameter measurement uncertainties (*e.g* [9, 10, 11]). This is due to the fact that these approaches do not trace the underlying physical mechanisms of measurements errors. Instead, these typical approaches follow an *empirical* paradigm in which S-parameter measurement uncertainties are obtained based on some approximate estimates of errors in S-parameters of calibration standards and raw VNA measurements.

In our approach, we follow a *physical* paradigm. We begin with the identification of all of the fundamental statistically independent physical error mechanisms in the VNA measurement. We then characterize these mechanisms with frequency-dependent physical models. Based on these models we determine the contribution of these error mechanisms to the VNA measurement uncertainty for all measurement frequencies and S-parameters at the same time. Consequently, we can readily determine all of the statistical correlations between these uncertainties and capture them with a covariance matrix.

## II. Physical Error Mechanisms

The notion of a physical error mechanism is fundamental to our covariance-based uncertainty analysis. It reflects the fact that the overall measurement error is caused by a set of fundamental physical error mechanisms. These error mechanisms correspond to both systematic measurement

Manuscript received November ..., 2009.

Arkadiusz Lewandowski is with the Warsaw University of Technology, Institute of Electronic Systems, Nowowiejska 15/19, 00-665 Warsaw, Poland (phone: +48 22 234 7877; e-mail: A.Lewandowski@ ieee.org).

Dylan F. Williams, Paul D. Hale, Jack C. M. Wang, and Andrew Dienstfrey are with the National Institute of Standards and Technology, 325 Broadway, Boulder, CO 80305, USA

* This work is a publication of the National Institute of Standards and Technology (NIST), an agency of the U.S. government, and is not subject to U.S. copyright.

errors (*e.g.*, uncertainties of dimensional and material parameters of the calibration standards) and random measurement errors (*e.g.*, bending of the cables, misalignment of inner and outer conductors, or displacements of the inner conductor fingers in coaxial connectors).

We represent a physical error mechanism with a *scalar random variable* $\xi$ that describes the variability of an underlying physical parameter characterizing this mechanism, and with a *physical model* that describes the relationship between this physical parameter and the corresponding error in S-parameter measurement. This relationship is determined by the electrical models of the calibration standards and the VNA instrumentation, and the mathematical description of the VNA calibration and correction procedure.

As the random parameter $\xi$ describes *changes*, we assume that it has a zero mean value and a variance $\sigma_\xi^2$. Typically, this parameter has a Gaussian or uniform probability density function. We further define the physical model representing the error mechanism as a vector function,

$$\Delta\mathbf{s} = \mathbf{m}(\xi), \tag{1}$$

where $\Delta\mathbf{s}$ is the error in S-parameter measurement $\mathbf{s}$. Both $\Delta\mathbf{s}$ and $\mathbf{s}$ are real-valued vectors with real and imaginary parts of corresponding S-parameters. These vectors have $Q = 2N^2K$ elements, where $N$ is the number of ports of the device under test (DUT) and $K$ is the number of measurement frequencies. The particular ordering of S-parameters in $\Delta\mathbf{s}$ and $\mathbf{s}$ is arbitrary and is not relevant for the following discussion.

## III. Covariance Matrix

The statistical properties of the physical error mechanisms can be conveniently captured in a covariance matrix

$$\mathbf{\Sigma}_\xi = \begin{bmatrix} \sigma_{\xi_1}^2 & & \\ & \ddots & \\ & & \sigma_{\xi_M}^2 \end{bmatrix}, \tag{2}$$

where $M$ is the number of mechanisms. Matrix (2) is diagonal, because the physical error mechanisms are statistically independent.

In order to determine the statistical properties of the error $\Delta\mathbf{s}$ in S-parameter measurement, we need to propagate the variability of the random parameters $\xi$ through the physical model (1). This model is, in general, nonlinear. However, since $\xi$ and $\Delta\mathbf{s}$ describe changes, we can assume that both variables are small. Consequently, we can linearize (1) and apply the superposition rule. The overall error in S-parameter measurement $\mathbf{s}$ is then written as a linear combination

$$\Delta\mathbf{s} = \mathbf{J}_\mathbf{m}\boldsymbol{\xi}, \tag{3}$$

where $\boldsymbol{\xi} = [\xi_1, \ldots, \xi_M]^T$ is a vector of random parameters representing the physical error mechanisms, and matrix $\mathbf{J}_\mathbf{m}$ is the Jacobian matrix defined by

$$\mathbf{J}_\mathbf{m} = \left.\frac{\partial \mathbf{m}(\boldsymbol{\xi})}{\partial \boldsymbol{\xi}^T}\right|_{\boldsymbol{\xi}=0} = \begin{bmatrix} \left.\frac{\partial m_1(\boldsymbol{\xi})}{\partial \xi_1}\right|_{\xi_1=0} & \cdots & \left.\frac{\partial m_1(\boldsymbol{\xi})}{\partial \xi_M}\right|_{\xi_M=0} \\ \vdots & \ddots & \vdots \\ \left.\frac{\partial m_Q(\boldsymbol{\xi})}{\partial \xi_1}\right|_{\xi_1=0} & \cdots & \left.\frac{\partial m_Q(\boldsymbol{\xi})}{\partial \xi_M}\right|_{\xi_M=0} \end{bmatrix}, \tag{4}$$

whose elements are the sensitivities of S-parameter measurement $\mathbf{s}$ to individual error mechanisms in $\boldsymbol{\xi}$. By use of (3) and (4) we then readily obtain the covariance matrix $\mathbf{\Sigma}_\mathbf{s}$ of error $\Delta\mathbf{s}$ in S-parameter measurement $\mathbf{s}$ as [12]

$$\mathbf{\Sigma}_\mathbf{s} = E\left[\Delta\mathbf{s}\Delta\mathbf{s}^T\right] = \mathbf{J}_\mathbf{m} E\left[\boldsymbol{\xi}\boldsymbol{\xi}^T\right]\mathbf{J}_\mathbf{m}^T = \mathbf{J}_\mathbf{m}\mathbf{\Sigma}_\xi\mathbf{J}_\mathbf{m}^T, \tag{5}$$

where $E[\cdot]$ is the expectation value operator [12]. In order to make sure that the linear approximation (5) holds, we verify it with numerical Monte Carlo simulations.

Matrix (5) contains a wealth of information. Its diagonal elements describe the variance of real and imaginary parts of the error in the corresponding S-parameters in the vector $\mathbf{s}$. The off-diagonal terms in $\mathbf{\Sigma}_\mathbf{s}$ correspond to all possible statistical correlations between these errors. In particular, these terms account for correlations between errors in S-parameter measurements at different frequencies.

We further note that for $Q \le M$ it is possible for matrix (5) to be full rank; however, for $Q > M$ the rank of matrix (5) is necessarily less than $Q$, hence its rows and columns are linearly dependent. This has an important implication. In practice $Q$ is usually much larger than $M$, because we measure S-parameters for a large number of frequencies. Consequently, we observe the variability of $Q$ random variables that results from only $M$ independent physical random mechanisms. Therefore, some fixed deterministic relationships between the variables in $\Delta\mathbf{s}$ exist, which are captured in the matrix $\mathbf{J}_\mathbf{m}$. As a result, instead of directly estimating the matrix $\mathbf{\Sigma}_\mathbf{s}$ based on repeated measurements, which is difficult because of a large number of variables [12, 13], it is more efficient to identify the underlying independent error mechanism $\boldsymbol{\xi}$ and the matrix $\mathbf{J}_\mathbf{m}$ whose columns capture the physical relationships between these error mechanisms and the measurement error.

Equation (5) also suggests another convenient form for representing the information captured in $\mathbf{\Sigma}_\mathbf{s}$. Let the square root $\boldsymbol{\sigma}_\xi$ of covariance matrix $\mathbf{\Sigma}_\xi$ be defined by

$$\mathbf{\Sigma}_\xi = \boldsymbol{\sigma}_\xi\boldsymbol{\sigma}_\xi. \tag{6}$$

Since the physical error mechanisms are uncorrelated, $\mathbf{\Sigma}_\xi$ is diagonal, and its square root matrix is also a diagonal matrix containing the square roots (standard deviations) of the variances in $\mathbf{\Sigma}_\xi$. With the use of $\boldsymbol{\sigma}_\xi$ we can now rewrite (5) as

$$\mathbf{\Sigma}_\mathbf{s} = \mathbf{J}_\mathbf{m}\Sigma_\xi\mathbf{J}_\mathbf{m}^T = \left(\mathbf{J}_\mathbf{m}\boldsymbol{\sigma}_\xi\right)\left(\mathbf{J}_\mathbf{m}\boldsymbol{\sigma}_\xi\right)^T = \mathbf{J}_\sigma\mathbf{J}_\sigma^T. \tag{7}$$

Thus, we can uniquely represent the $Q \times Q$ matrix $\mathbf{\Sigma}_\mathbf{s}$ with a

much smaller $Q \times M$ matrix $\mathbf{J}_\sigma$ made up of columns of $\mathbf{J_m}$ multiplied by standard deviations of error mechanisms in $\boldsymbol{\xi}$.

## IV. Propagating Covariance-Matrix-Based Uncertainties

In this section we review the propagation of covariance-based uncertainties into the uncertainties of quantities derived from S-parameter measurements. We focus here on a general case when the quantity derived from S-parameters depends on measurements of S-parameters for *all* frequencies. Cases, for which the derived quantities depend on S-parameters at only *one* frequency have already been discussed in the literature [7].

There are many practical situations when we need to derive some quantities from S-parameter measurements performed for multiple frequencies. Examples here are the transformation of the reflection coefficient into the time-domain in VNA-based time-domain reflectometry, or the mismatch correction in oscilloscope measurements. Other examples are measurement-based circuit modeling, such as determining the equivalent circuit of a transistor from S-parameter measurements.

In all of these cases we can represent the relationship between S-parameter measurements and the derived quantities as a vector function

$$\mathbf{y} = \mathbf{f}(\mathbf{s}), \quad (8)$$

where $\mathbf{y}$ is vector of derived quantities, and $\mathbf{s}$ is the S-parameter measurement vector[†]. For a given measurement $\mathbf{s}_0$ of S-parameters, we assume that $\mathbf{f}(\mathbf{s})$ is differentiable in $\mathbf{s}_0$ and approximate it with a first-order Taylor expansion of (8) around $\mathbf{s}_0$, that is ,

$$\mathbf{y} \approx \mathbf{f}(\mathbf{s}_0) + \mathbf{J_f}\Delta\mathbf{s}, \quad (9)$$

where $\Delta\mathbf{s}$ is the measurement error in $\mathbf{s}$ and $\mathbf{J_f}$ is the Jacobian matrix of partial derivatives, defined as

$$\mathbf{J_f} = \left.\frac{\partial \mathbf{f}(\mathbf{s})}{\partial \mathbf{s}^T}\right|_{\mathbf{s}=\mathbf{s}_0}, \quad (10)$$

which has a similar form to (4). We then insert (5) in (9) and determine the covariance matrix as

$$\boldsymbol{\Sigma}_\mathbf{y} \approx \mathrm{E}\left[\mathbf{J_f}\Delta\mathbf{s}\left(\mathbf{J_f}\Delta\mathbf{s}\right)^T\right] = \mathbf{J_f}\mathrm{E}\left[\Delta\mathbf{s}\Delta\mathbf{s}^T\right]\mathbf{J_f}^T = \mathbf{J_f}\boldsymbol{\Sigma}_\mathbf{s}\mathbf{J_f}^T. \quad (11)$$

Expression (11) gives us an approximation of the covariance matrix of the quantity derived from S-parameter measurements. When $\mathbf{f}(\mathbf{s})$ is linear, equation (11) is exact. For a function that is nonlinear, approximation (11) holds as long as $\mathbf{f}(\mathbf{s})$ is differentiable at $\mathbf{s}_0$ and errors in S-parameter measurement are small relative to neglected nonlinear terms. In the case when $\mathbf{f}(\mathbf{s})$ is highly nonlinear or errors are large, a numerical Monte Carlo simulation may be necessary to obtain $\boldsymbol{\Sigma}_\mathbf{y}$.

[†] The derived quantities may also depend on some quantities other than S-parameters; however, for the sake of simplicity, we do not explicitly account for this dependence in our notation.

Equation (11) shows that both covariance matrices $\boldsymbol{\Sigma}_\mathbf{y}$ and $\boldsymbol{\Sigma}_\mathbf{s}$ are closely related. In the case when each element of $\mathbf{y}$ depends on S-parameter measurements at only *one* frequency, the Jacobian matrix $\mathbf{J_f}$ has a block diagonal form. Consequently, correlations between S-parameter measurement uncertainties for different frequencies do not affect $\boldsymbol{\Sigma}_\mathbf{y}$. However, when elements of $\mathbf{y}$ depend on S-parameter measurement uncertainties for *all* frequencies, such as in the case of conversion from the frequency domain into the temporal domain, the Jacobian matrix $\mathbf{J_f}$ is dense and correlations between S-parameter measurements uncertainties contribute to both variances and covariances in $\boldsymbol{\Sigma}_\mathbf{y}$.

We can put (11) in a different form by use of (7). We then obtain

$$\boldsymbol{\Sigma}_\mathbf{y} \approx \mathbf{J_f}\boldsymbol{\Sigma}_\mathbf{s}\mathbf{J_f}^T = \left(\mathbf{J_f}\mathbf{J}_\sigma\right)\left(\mathbf{J_f}\mathbf{J}_\sigma\right)^T. \quad (12)$$

This relationship suggests that we can perform the uncertainty propagation entirely by use of Jacobian matrices with columns scaled by the standard uncertainties of the physical error mechanisms. Consequently, we may evaluate the full covariance matrix of derived quantities only at the last step of the uncertainty propagation.

## V. Reporting Covariance-Matrix-Based Uncertainties

Covariance-matrix $\boldsymbol{\Sigma}_\mathbf{y}$ describes the measurement uncertainty in vector $\mathbf{y}$ representing the quantity derived from S-parameter measurement (or, in the simplest case, the S-parameter measurement itself). When reporting the uncertainty captured in $\boldsymbol{\Sigma}_\mathbf{y}$, as in the scalar case, we are typically interested in the confidence region. Assuming that $\boldsymbol{\Sigma}_\mathbf{y}$ is full rank, this region is defined as a multidimensional ellipsoid around the estimate $\hat{\mathbf{y}}$ of $\mathbf{y}$ within which we expect, with a prescribed likelihood $1-\alpha$, the true value of $\mathbf{y}$ to lie [12, 13]. This confidence region can be written as

$$\left(\mathbf{y}-\hat{\mathbf{y}}\right)^T \boldsymbol{\Sigma}_\mathbf{y}^{-1}\left(\mathbf{y}-\hat{\mathbf{y}}\right) \le T^2_{M,P,1-\alpha}, \quad (13)$$

where $T^2_{\nu,p,1-\alpha}$ is the $1-\alpha$ quintile of Hotteling's $T^2$ distribution with $\nu$ and $p$ degrees of freedom [12, 13], $M$ is the number of physical error mechanisms, and $P$ is the number of elements in the vector $\mathbf{y}$.

When evaluating (13), we need to pay special attention to the rank of $\boldsymbol{\Sigma}_\mathbf{y}$. As already mentioned, the variability of $\mathbf{y}$ results from a finite number of $M$ physical error mechanisms. We determine this number based on the number of columns in the $\mathbf{J}_\sigma$ matrix used to construct $\boldsymbol{\Sigma}_\mathbf{y}$. When $M$ is smaller than the size $P$ of the vector $\mathbf{y}$, the covariance matrix $\boldsymbol{\Sigma}_\mathbf{y}$ becomes rank deficient and cannot be inverted. Consequently, (13) is no longer valid. In this case, the confidence region needs to be defined in terms of physical mechanisms rather than measured quantities and then mapped into the domain of

$\mathbf{y}$. This is, however, beyond the scope of this paper.

In practice we are often interested in the uncertainties of only single elements of the vector $\mathbf{y}$. Examples are real and imaginary part, or magnitude and phase, of an S-parameter at a particular frequency, or waveform voltage at a particular time-point. The confidence region then reduces to a typical one-dimensional confidence interval [14]. Denoting this element by $y$ and its estimate by $\hat{y}$, we can write the confidence interval as

$$-t_{M,1-\alpha} \leq \frac{y-\hat{y}}{\sigma_y} \leq t_{M,1-\alpha}, \tag{14}$$

where $t_{\nu,1-\alpha}$ is the $1-\alpha$ quintile of the Student's $t$-distribution with $\nu$ degrees of freedom [14].

## VI. Uncertainty Analysis for VNA Measurement

Our uncertainty analysis for VNA S-parameter measurements is based on the covariance-matrix description introduced in Section III. We perform our analysis in two steps. In the first step, we carefully identify all of the independent physical sources of measurement errors. As a result of this step we obtain the variances of these mechanisms, as captured in matrix $\mathbf{\Sigma}_{\xi}$. In the second step, we determine how these mechanisms affect corrected S-parameter measurements at *all* frequencies and represent this information with the matrix $\mathbf{J}_{\sigma}$ as defined by (7). This matrix allows us to eventually determine the covariance matrix $\mathbf{\Sigma}_{\mathbf{s}}$.

We divide the error mechanisms into two groups: calibration standard errors and VNA instrumentation errors. The calibration standard errors result from uncertainties in the dimensional and material parameters of the calibration standards. The VNA instrumentation errors are caused primarily by the connector nonrepeatability and cable instability. We write the overall error in S-parameter measurement as a sum

$$\Delta\mathbf{s} = \mathbf{J}_{STD}\boldsymbol{\xi}_{STD} + \mathbf{J}_{VNA}\boldsymbol{\xi}_{VNA}, \tag{15}$$

where $\boldsymbol{\xi}_{STD}$ and $\boldsymbol{\xi}_{VNA}$ are vectors of random variables corresponding to physical parameters that characterize the calibration standard and VNA instrumentation error mechanisms, respectively, and $\mathbf{J}_{STD}$ and $\mathbf{J}_{VNA}$ are the corresponding Jacobian matrices, defined by (4). These matrices capture the transformation between changes in the physical parameters in $\boldsymbol{\xi}_{STD}$ and $\boldsymbol{\xi}_{VNA}$ and the resulting error $\Delta\mathbf{s}$ in the frequency-dependent S-parameter measurement $\mathbf{s}$. In the following we discuss the approach we employed to obtain the representation (15).

### A. *Calibration standard errors*

In order to identify the calibration-standard error-mechanisms, we begin with physical modeling of the calibration standards. The goal of this modeling is to express S-parameters of calibration standards in terms of some fundamental dimensional and material parameters. Examples here are lengths and diameters of conductors in the coaxial transmission line. Such models for different calibration standards have been extensively discussed in the literature (*e.g.*, see [15] and [16]); we will not discuss them in more detail.

TABLE I
Physical Parameters of 1.85 MM Coaxial Transmission Lines

| Parameter† | Value [mm] | Standard uncertainty [ $\mu$ m] |
|---|---|---|
| Line 1 OC length | 29.981 | 5 |
| Line 2 OC length | 23.066 | 5 |
| Line 3 OC length | 18.573 | 5 |
| Line 4 OC length | 16.337 | 5 |
| Line 5 OC length | 14.999 | 5 |
| Line 1 IC length | 29.971 | 5 |
| Line 2 IC length | 23.060 | 5 |
| Line 3 IC length | 18.572 | 5 |
| Line 4 IC length | 16.331 | 5 |
| Line 5 IC length | 14.991 | 5 |
| Line 1 OC diameter | 1.8499 | 0.6 |
| Line 2 OC diameter | 1.851 | 1 |
| Line 3 OC diameter | 1.8503 | 0.6 |
| Line 4 OC diameter | 1.852 | 1 |
| Line 5 OC diameter | 1.8518 | 0.6 |
| Line 1 IC diameter | 0.803 | 5 |
| Line 2 IC diameter | 0.804 | 6 |
| Line 3 IC diameter | 0.805 | 7 |
| Line 4 IC diameter | 0.804 | 6 |
| Line 5 IC diameter | 0.804 | 6 |

†IC - inner conductor, OC -outer conductor

In the next step, we measure these fundamental dimensional parameters. For example, in the case of coaxial calibration standards used in this work, such measurements involve the use of precision air gages and mechanical blocks. The uncertainties of these measurements then become the estimates of standard deviations of calibration-standard error-mechanisms in $\boldsymbol{\xi}_{STD}$. In order to determine the columns of matrix $\mathbf{J}_{STD}$, we then use the rules described in Section IV to propagate these uncertainties through the physical models of the calibration standards and the VNA calibration and correction procedure. We use the flexible calibration approach of [17] which allows us to easily adjust our uncertainty analysis to an arbitrary calibration procedure.

We illustrate this with the multiline TRL calibration [18] in the 1.85 mm coaxial connector standard. This calibration employed a set of five insertable airlines, a flat short as the reflect standard, and the direct connection of test ports as the thru standard. The only systematic errors in our calibration result from the Type B uncertainties for the lengths and diameters of 1.85 mm airline standards, which are listed in Table I. We derived these uncertainties from the specifications of the air-gage and mechanical blocks used to measure the airlines.

### B. *VNA instrumentation errors*

A covariance-matrix based description of VNA instrumentation errors poses a more complex problem than the evaluation of calibration standard errors. It is difficult, in practice, to characterize the VNA instrumentation errors with analytical models derived from fundamental mechanical and electrical parameters of the VNA. For example, in the case of

connector repeatability errors, this would require careful mechanical characterization of *all* of the possible mechanical displacements in the connector interface, and then electro-mechanical modeling of their influence on the interface S-parameters. Although such an approach has been applied to simplified connector models (*e.g.*, see [19] and [20]), the real connector structures are extremely difficult to model . The situation is even more difficult with the random errors caused by cable instability or test-set drift. Analytical modeling of electrical parameters of such complex structures is beyond our capacity.

Hence, our approach to the description of VNA instrumentation errors is different and is based on behavioral stochastic modeling. We begin with the generic physical model for the VNA random errors proposed in [21], and shown schematically in Fig. 1. This model describes the frequency-dependence of VNA random errors with a set of lumped-element perturbations located at fixed distances within the VNA error box. Based on that description, we build a stochastic model in which parameters of the perturbations may vary randomly. We then identify statistical properties of these parameters based on repeated measurements. In this way, we represent the complicated frequency-dependent behavior of VNA instrumentation errors with a very small set of frequency-independent random variables $\xi_{VNA}$ and some fixed functions that capture the frequency dependence of these errors. These functions stem from the structure of the model shown in Fig. 1; for more details refer to [21]. Similarly to the calibration standard errors, we then determine the columns of the matrix $\mathbf{J}_{VNA}$ by propagating these functions through the VNA calibration and correction procedure with the use the rules described in Section IV.

In order to identify statistical properties of $\xi_{VNA}$, we use repeated measurements. In the case of connector repeatability errors, we perform multiple reflection coefficient measurements of a highly reflective load while reconnecting the load between the measurements. In the case of cable instability errors, we proceed in a similar way; however, instead of reconnecting the load, we randomly bend the cable between the measurements.

For a given sample of repeated measurements $\mathbf{s}_i$, for $i = 1,\ldots,R$, we first determine the mean $\overline{\mathbf{s}}$ and calculate the estimates $\Delta\mathbf{s}_i = \mathbf{s}_i - \overline{\mathbf{s}}$ of the measurement error. We use the model-identification approach presented in [21] to determine the parameters $\xi_{VNA,i}$ that model the measurement error $\Delta\mathbf{s}_i$, and then determine the sample covariance matrix $\mathbf{\Sigma}_{\xi_r}$ for the parameters $\xi_{VNA,i}$, for $i = 1,\ldots,R$. We further apply principal component analysis (see [12]) to diagonalize this matrix and reduce its dimensionality while capturing the most important error mechanisms in the system. As a result, we are usually able to adequately represent the connector repeatability and cable instability errors with only two or three random variables.

In Fig. 2, we illustrate our approach with modeling results for the connector repeatability errors. This figure shows the in-phase and quadrature component (see [22]) of the standard uncertainty of 16 repeated measurements of a 5.4 mm long 1.85 mm coaxial offset short along with the uncertainty prediction from our stochastic behavioral model. We took the measurements for a narrow intermediate-frequency bandwidth of 10 Hz in order to reduce the noise impact. For this reason, the 16 repeated measurements took approximately 30 minutes.

The model we used employed two random variables. The agreement between the model prediction and measurement for the quadrature (phase) errors is very good except for a small discrepancy in the frequency range below 4 GHz. This discrepancy is caused by an increased test-set drift in the frequency range below 4 GHz, a phenomenon we also noticed in other experiments.

The agreement for the in-phase (magnitude) errors is not as good; however, the in-phase errors are much smaller, and therefore less important than the quadrature errors. Consequently, our stochastic behavioral model is capable of adequately representing the dominant variability of the connector interface observed in the measurements of the short.

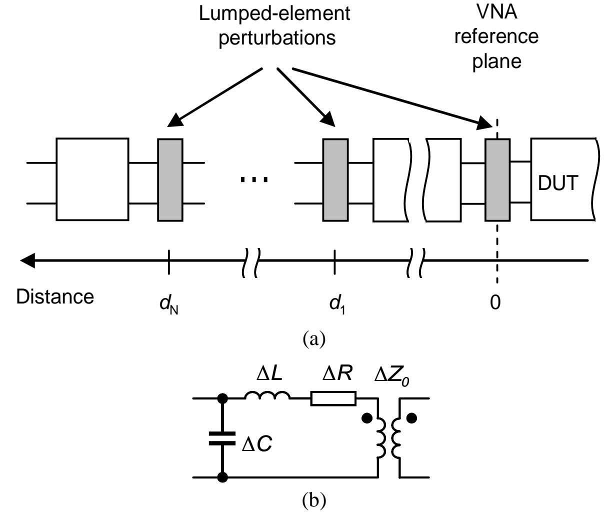


Fig. 1. Behavioral physical model for VNA random errors: (a) overview, (b) single perturbation.

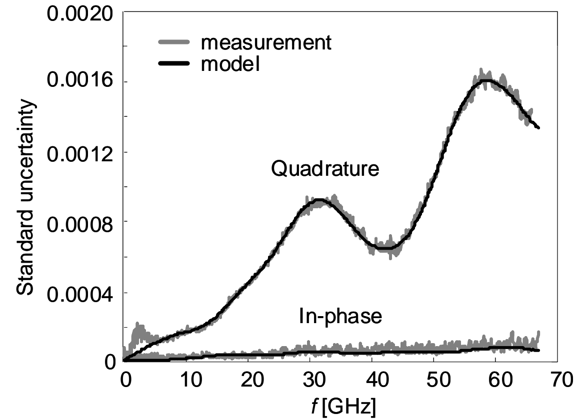


Fig. 2. In-phase and quadrature component of the standard uncertainty of 16 measurements of a 5.4 mm long 1.85 mm coaxial offset short: measurement (grey) and stochastic behavioral model prediction (black).

## VII. Application Examples

### A. Mismatch-correcting waveform measurements

Measurement of waveforms with bandwidths reaching microwave frequencies are typically performed with high-speed sampling oscilloscopes. Unlike their low-frequency counterparts, these oscilloscopes are designed to be connected directly to the circuit under test and to measure the voltage the circuit generates across the oscilloscope's 50 Ω input impedance [23]. Accuracy of such measurements can be improved if the impedance mismatch between the circuit-under-test and the oscilloscope is accounted for. This is typically done by measuring the DUT and oscilloscope impedance with the VNA and applying an appropriate correction to the waveform measured by the oscilloscope [23]. Here, we will show that the uncertainty analysis of such mismatch-corrected waveform measurements requires a full covariance-matrix description of the uncertainties in VNA measurements.

Fig. 3 shows the signal-flow graph that models the propagation of the signal between the DUT and the oscilloscope [23]. The DUT generates the signal with the forward-wave voltage $v_{DUT} = \sqrt{50\,\Omega}\, b_{DUT}$, where $b_{DUT}$ is the forward-wave source amplitude, and the oscilloscope measures the voltage $v_s = \sqrt{50\,\Omega}\, a_s$ corresponding to the wave amplitude $a_s$. We can write the relationship between the two voltages as [23]

$$v_{DUT} = v_s \frac{1-\Gamma_s \Gamma_{DUT}}{h}, \tag{16}$$

where $\Gamma_s$ is the input reflection coefficient of the oscilloscope and $h$ is the oscilloscope's complex frequency response (*i.e.*, the Fourier transform of its impulse response) ‡.

In order to perform the uncertainty analysis of (16) we use the uncertainty propagation rules described in Section IV. Here, we focus only on the uncertainty components due to the errors in VNA measurements. A complete uncertainty analysis, however, also needs to account for errors in the oscilloscope's raw measurement $v_s$ and the oscilloscope's complex frequency response $h$.

We represent the reflection coefficient measurement of the oscilloscope and DUT as vectors $\mathbf{\Gamma}_{DUT}$ and $\mathbf{\Gamma}_s$, respectively, and the waveform spectrum of the DUT as vector $\mathbf{v}_{DUT}$. These vectors are constructed out of measurements for all frequencies, that is

‡ Equation (16) is suitable when the frequency content of the signals is within the bandwidth of the oscilloscope, *i.e.*, $|h|$ is roughly a unit magnitude. At high frequencies, as $|h|$ rolls off, (16) is ill-posed and cannot be directly used to determine $v_{DUT}$. Regularization techniques need to be then used (see [3]).

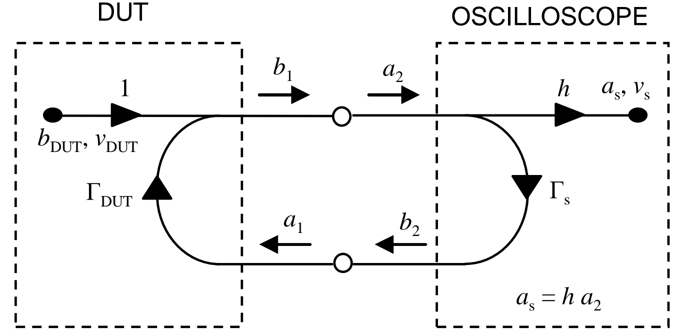


Fig. 3. Signal-flow graph describing the propagation of signals between the DUT and oscilloscope. The DUT injects into the circuit the signal $b_{DUT}$ with no distortion, as indicated by the unity transfer function. The signal delivered to the oscilloscope is modified by the transfer function , as well as being reflected multiple times by $\Gamma_s$ and $\Gamma_{DUT}$.

$$\mathbf{\Gamma}_{DUT} = \begin{bmatrix} \Gamma_{DUT}(0) \\ \Gamma_{DUT}(f_1) \\ \vdots \\ \Gamma_{DUT}(f_N) \end{bmatrix}, \mathbf{\Gamma}_s = \begin{bmatrix} \Gamma_s(0) \\ \Gamma_s(f_1) \\ \vdots \\ \Gamma_s(f_N) \end{bmatrix}, \text{and } \mathbf{v}_{DUT} = \begin{bmatrix} v_{DUT}(0) \\ v_{DUT}(f_1) \\ \vdots \\ v_{DUT}(f_N) \end{bmatrix},$$

where $f_i$, for $i = 0,\ldots,N$ are the measurement frequencies, and $f_0 = 0$. Similarly, we represent the temporal waveforms $V_s(t_i)$ and $V_{DUT}(t_i)$, where $t_i$ for $i = 1,\ldots,2N$ are the time points, as vectors made up of measurements for all time points, that is

$$\mathbf{V}_{DUT} = \begin{bmatrix} V_{DUT}(t_1) \\ \vdots \\ V_{DUT}(t_{2N}) \end{bmatrix}, \text{and } \mathbf{V}_s = \begin{bmatrix} V_s(t_1) \\ \vdots \\ V_s(t_{2N}) \end{bmatrix}.$$

Since the spectra are determined for $N+1$ frequencies, the corresponding waveforms have $2N$ time points [24].

With the use of (11) we can write the covariance matrix of the waveform spectrum as

$$\mathbf{\Sigma}_{\mathbf{v}_{DUT}} = \mathbf{J}_{\mathbf{\Gamma}_s} \mathbf{\Sigma}_{\mathbf{\Gamma}_s} \mathbf{J}_{\mathbf{\Gamma}_s}^T + \mathbf{J}_{\mathbf{\Gamma}_{DUT}} \mathbf{\Sigma}_{\mathbf{\Gamma}_{DUT}} \mathbf{J}_{\mathbf{\Gamma}_{DUT}}^T, \tag{17}$$

where $\mathbf{\Sigma}_{\mathbf{\Gamma}_s}$ and $\mathbf{\Sigma}_{\mathbf{\Gamma}_{DUT}}$ are the covariance matrices of the oscilloscope's input reflection coefficient and the DUT's reflection coefficient, respectively, and $\mathbf{J}_{\mathbf{\Gamma}_s}$ and $\mathbf{J}_{\mathbf{\Gamma}_{DUT}}$ are the Jacobian matrices. The uncertainty of the DUT waveform spectrum at a particular frequency depends on only the uncertainties of reflection coefficient measurements for that same frequency; hence matrices $\mathbf{J}_{\mathbf{\Gamma}_s}$ and $\mathbf{J}_{\mathbf{\Gamma}_{DUT}}$ are block diagonal and consist of first derivatives of (16) with respect to $\Gamma_s$ and $\Gamma_{DUT}$, evaluated at each measurement frequency. However, the matrices $\mathbf{\Sigma}_{\mathbf{\Gamma}_s}$ and $\mathbf{\Sigma}_{\mathbf{\Gamma}_{DUT}}$ are dense, and consequently the covariance matrix $\mathbf{\Sigma}_{\mathbf{v}_{DUT}}$ is also dense.

In order to determine the uncertainty of the DUT temporal waveform we need to use the discrete inverse Fourier transform. This transform is a linear operation, hence the relationship between DUT waveform spectrum and its temporal representation can be written as

$$\mathbf{V}_{DUT} = \mathbf{M}\mathbf{v}_{DUT} , \tag{18}$$

where $\mathbf{M}$ is the matrix of the Fourier series coefficients. This matrix is dense, because a single time-domain sample is a function of all spectrum components. By use of (18) and (11) we can write

$$\mathbf{\Sigma}_{\mathbf{V}_{DUT}} = \mathbf{M}\left(\mathbf{J}_{\Gamma_s}\mathbf{\Sigma}_{\Gamma_s}\mathbf{J}_{\Gamma_s}^T + \mathbf{J}_{\Gamma_{DUT}}\mathbf{\Sigma}_{\Gamma_{DUT}}\mathbf{J}_{\Gamma_{DUT}}^T\right)\mathbf{M}^T . \tag{19}$$

Expression (19) is a very important result. Simple investigation shows that the uncertainties of waveform amplitudes depend both on uncertainties in S-parameter measurements and on statistical correlations between these uncertainties at different frequencies. Therefore estimation of these correlations is essential when VNA S-parameter measurements are used in the calibration of waveform measurement systems.

In order to illustrate the importance of these correlations, we performed an experiment. We measured a pulse generated by a photodiode with a 50 GHz sampling oscilloscope and from that we determined the mismatch-corrected impulse response of the oscilloscope by means of the approach of [2]. Both the photodiode and the oscilloscope had 1.0 mm coaxial connectors. The output reflection coefficient of the pulse generator and the input reflection coefficient of the oscilloscope were measured with a VNA calibrated with the use of 1.0 mm coaxial short-open-load-through (SOLT) calibration. The covariance matrix of uncertainties in S-parameters was determined with the methods discussed in Section VI. We then analyzed the impact of mismatch correction uncertainty on the impulse response uncertainties. We analyzed two different cases: when the uncertainties in the mismatch-corrected impulse response are determined accounting for the correlations between uncertainties for different frequencies, and when these correlations are neglected. Results of our experiment are shown in Fig. 4. We see that when the statistical correlations between the uncertainties are accounted for, the standard uncertainty (solid grey line) in the corrected waveform (solid black line) approximately follows the shape of the waveform. In particular, we note increased measurement uncertainty around the impulse response peak. When these correlations are neglected, the uncertainties (dashed grey line) are uniformly spread over the duration of the impulse response. Consequently, the uncertainties away from the impulse response peak are overestimated, while the uncertainties around the peak are underestimated.

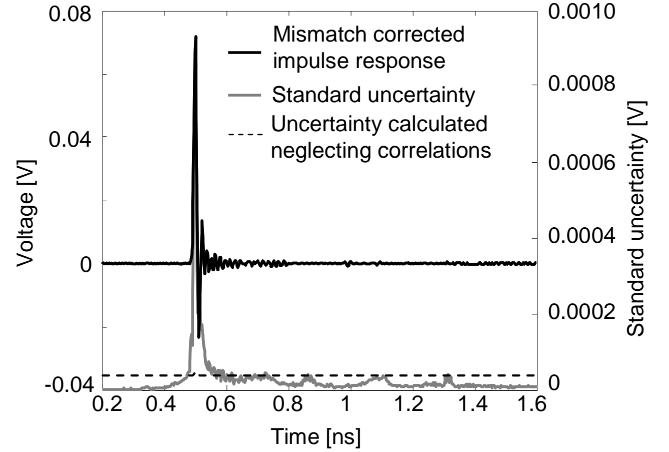


Fig. 4. Uncertainty analysis of the mismatch correction in oscilloscope waveform measurement: pulse voltage after the mismatch correction (solid black), standard uncertainty of the pulse voltage (solid grey), standard uncertainty of the pulse voltage calculated without correlations (dashed grey).

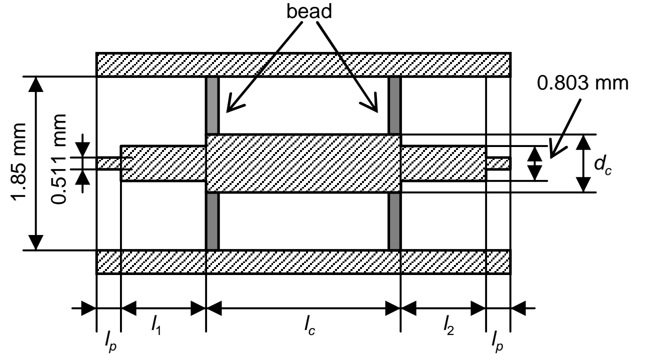


Fig. 5. Schematic of the 1.85 mm coaxial mismatch thru. Dimensions with numerical values are fixed and taken from [28]; other dimensions are estimated in the modeling procedure.

## *B. Measurement-based modeling*

In the measurement-based modeling we determine an electrical model of a device based on a measurement of its electrical characteristics, such as a wideband VNA S-parameters measurement. Examples include modeling of active devices, such as microwave transistors, and passive devices, such as transmission line discontinuities [25].

A number of different approaches are used in the measurement-based modeling. These approaches are typically based on a statistical formulation of the modeling problem and employ numerical optimization techniques to determine model parameters from VNA S-parameter measurements of the device [26]. In the context of uncertainty analysis, we can write the modeling procedure as a function that transforms the VNA S-parameter measurement $\mathbf{s}$ into model parameters $\mathbf{p}$, that is,

$$\mathbf{p} = \mathbf{f}\left(\mathbf{s}\right) . \tag{20}$$

Parameters in the vector $\mathbf{p}$ are typically frequency independent (*e.g.* capacitances, inductances of resistances of an equivalent circuit), while the vector $\mathbf{s}$ contains measurement of S-parameters for multiple frequencies. The particular form of the function $\mathbf{f}$ depends on the formulation of the modeling problem and methods used to solve it.

In order to determine the covariance matrix $\mathbf{\Sigma}_{\mathbf{p}}$ of model parameters we may now apply the uncertainty propagation rules described in Section IV to (20). Since each model parameter depends on S-parameter measurement at *all* frequencies, the uncertainties of model parameters will depend on statistical correlations between uncertainties in S-parameter measurement at different frequencies.

We illustrate this with an example of measurement-based

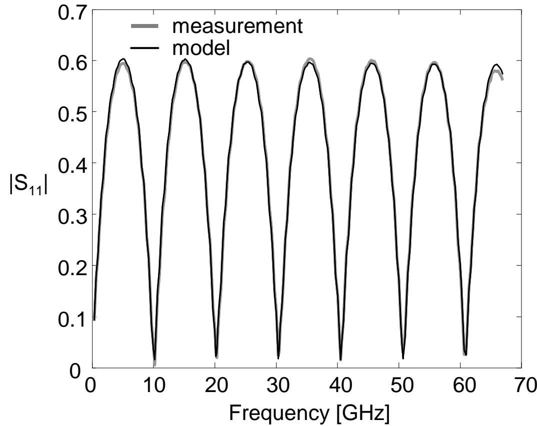


Fig. 6. Modeling of the 1.85 mm coaxial mismatch thru: magnitude of $S_{11}$, measurement (solid grey), model (solid black).

TABLE II
PARAMETERS OF 1.85 MM MISMATCH THRU MODEL

| Parameter | Value | Standard uncertainty | Standard uncertainty without correlations |
|---|---|---|---|
| $l_1$ [$\mu$m] | 5630 | 7 | 9 |
| $l_2$ [$\mu$m] | 5620 | 6 | 9 |
| $l_c$ [$\mu$m] | 14666 | 25 | 21 |
| $l_p$ [$\mu$m] | 30 | 7 | 5 |
| $\sigma$ [$10^7$ S/m] | 0.736 | 0.04 | 0.16 |
| $d_c$ [$\mu$m] | 1227 | 0.2 | 0.3 |
| $C_{joint}$ [fF] | 3.96 | 1.26 | 1.11 |
| $C_{gap}$ [fF] | 1.79 | 0.46 | 0.27 |

modeling for a 1.85 mm coaxial Beatty standard. This device is a section of low-impedance transmission line embedded in a nominally 50 Ω line. A schematic of this device, along with geometrical dimensions, is shown in Fig. 5. We model this device as a cascade of transmission lines with additional capacitances $C_{joint}$ and $C_{step}$ accounting for the connector joint discontinuity (see [27]), and the bead at the impedance step. We model the center conductor gap as a section of high impedance line (of fixed diameter 0.511 mm [28]) with length $l_p$. We assume that all lines exhibit conductor losses characterized by the metal conductivity $\sigma$.

We measured S-parameters of the device with the use of a VNA calibrated with the multiline TRL calibration. The measurements were performed in the frequency range 0.05-67 GHz. We obtained model parameters with the classical least-squares fitting [26] and then performed the uncertainty analysis with methods described in Section VI. In Fig. 6 and 7, we compare the magnitudes of $S_{11}$ and $S_{21}$ obtained from the measurement and from the model. The agreement is very good. In Table II, we show the model parameters obtained along with the standard uncertainties. We determined these uncertainties in two ways: with the use of the full covariance matrix and then by neglecting the correlations between S-parameter uncertainties for different frequencies. Results shown in Table II indicate that neglecting these correlations leads to very different estimates of the uncertainties on the model parameters. As in examples shown in Section VII.A, neglecting these correlations may cause both underestimation and overestimation of the uncertainties.

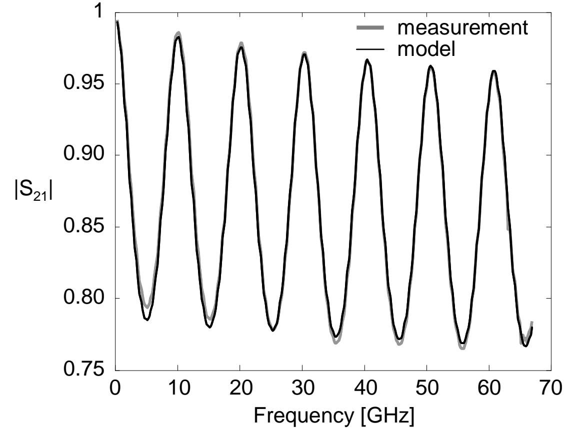


Fig. 7. Modeling of the 1.85 mm coaxial mismatch thru: magnitude of $S_{21}$, measurement (solid grey), model (solid black).

## VIII. CONCLUSIONS

We present a new uncertainty analysis for VNA S-parameter measurements. Our approach is based on a covariance-matrix uncertainty description that allows us to capture all of the S-parameter measurement uncertainties and statistical correlations between them. In particular, through a careful identification and modeling of underlying error mechanisms in VNA S-parameter measurements, we are able to determine the statistical correlations between uncertainties at different frequencies. Consequently, the covariance-based uncertainties of VNA S-parameter measurements we report can be propagated into the uncertainties of any other quantity derived from S-parameters.

We further showed that the correlations between uncertainties at different frequencies become important when converting S-parameter uncertainties into a domain different from the frequency-domain, such as when converting S-parameter uncertainties into the temporal domain or determining some frequency-independent parameters based on S-parameter measurements. We illustrated that with the uncertainty analysis of mismatch correction in waveform measurements and the uncertainty analysis of S-parameter-measurement-based modeling. In both cases the experimental results we obtained clearly demonstrate that accounting for the statistical correlations between S-parameter measurement uncertainties at different frequencies is essential for correct evaluation of uncertainties in quantities derived from S-parameter measurements.

## ACKNOWLEDGMENT

Arkadiusz Lewandowski thanks Prof. Janusz Dobrowolski for his continuous support and encouragement for this work.

## REFERENCES


[1] D. F. Williams, A. Lewandowski, T. S. Clement, J. C. M. Wang, P. D. Hale, J. M. Morgan, D. A. Keenan, and A. Dienstfrey, "Covariance-based uncertainty analysis of the NIST electrooptic sampling system," *IEEE Trans. Microw. Theory Tech.*, vol. 54, no. 1, pp. 481–491, 2006.

[2] T. S. Clement, P. D. Hale, D. F. Williams, C. M. Wang, A. Dienstfrey, and D. A. Keenan, "Calibration of sampling oscilloscopes with high-speed photodiodes," *IEEE Trans. Microw. Theory Tech.*, vol. 54, no. 8, pp. 3173–3181, Aug. 2006.

[3] P. D. Hale, A. Dienstfrey, J. Wang, D. F. Williams, A. Lewandowski, D. A. Keenan, and T. S. Clement, "Traceable waveform calibration with a covariance-based uncertainty analysis," *IEEE Trans. Instrum. Meas.*, vol. 58, no. 10, pp. 3554–3568, Oct. 2009.

[4] J. Verspecht, "Large-signal network analysis," *IEEE Microw. Mag.*, vol. 6, no. 4, pp. 82–92, Dec 2005.

[5] R. M. Judish and G. F. Engen, "On-line accuracy assessment for the dual six-port ANA: Statistical methods for random errors," *IEEE Trans. Instrum. Meas.*, vol. 36, pp. 507–513, 1987.

[6] C. A. Hoer, "On-line accuracy assessment for the dual six-port ANA: Treatment of systematic errors," *IEEE Trans. Instrum. Meas.*, vol. 36, pp. 514–523, 1987.

[7] N. M. Ridler and M. J. Salter, "Propagating S-parameter uncertainties to other measurement quantities," in $58^{th}$ *ARTFG Conf. Digest*, vol. 40, 2001, pp. 1–19.

[8] ——, "An approach to the treatment of uncertainty in complex S-parameter measurements," *Metrologia*, vol. 39, no. 3, pp. 295–302, 2002.

[9] D. K. Rytting, "Network analyzer accuracy overview," in $58^{th}$ *ARTFG Conf. Digest*, vol. 40, November 2001, pp. 1–13.

[10] U. Stumper, "Uncertainty of VNA S-parameter measurement due to nonideal TRL calibration items," *IEEE Trans. Instrum. Meas.*, vol. 54, no. 2, pp. 676–679, Apr 2005.

[11] *Guidelines on the evaluation of Vector Network Analyzers (VNA)*, July 2007, Doc. EURAMET/cg-12/v.01.

[12] D. F. Morrison, *Multivariate statistical methods*. McGraw-Hill, 1967.

[13] R. Willink and B. D. Hall, "A classical method for uncertainty analysis with multidimensional data," *Metrologia*, vol. 39, no. 4, pp. 361–369, 2002.

[14] *Guide to the Expression of Uncertainty in Measurement*, International Organization for Standarization, Genvea, 1993.

[15] K. H. Wong, "Characterization of calibration standards by physical measurements," in $39^{th}$ *ARTFG Conf. Digest*, vol. 21, June 1992, pp. 53–62.

[16] W. C. Daywitt, "First-order symmetric modes for a slightly lossy coaxial transmission line," *IEEE Trans. Microw. Theory Tech.*, vol. 38, no. 11, pp. 1644–1650, Nov. 1990.

[17] D. Williams, J. Wang, and U. Arz, "An optimal vector-network-analyzer calibration algorithm," *IEEE Trans. Microw. Theory Tech.*, vol. 51, no. 12, pp. 2391–2401, Dec. 2003.

[18] R. Marks, "A multiline method of network analyzer calibration," *IEEE Trans. Microw. Theory Tech.*, vol. 39, no. 7, pp. 1205–1215, July 1991.

[19] J. Miall and K. Lees, "Modeling the repeatability of Type-N connectors using Microwave Studio," in *Proc.* $19^{th}$ *ANAMET Meeting*, 2003.

[20] J. P. Hoffmann, P. Leuchtmann, and R. Vahldieck, "Pin gap investigations for the 1.85 mm coaxial connector," in *Proc. European Microwave Conference*, 9–12 Oct. 2007, pp. 388–391.

[21] A. Lewandowski and D. F. Williams, "Characterization and modeling of random vector-network-analyzer measurement errors," in $17^{th}$ *MIKON Conf. Digest*, May 19-21 2008.

[22] D. F. Williams, C. F. Wang, and U. Arz, "In-phase/quadrature covariance-matrix representation of the uncertainty of vectors and complex numbers," $68^{th}$ *ARTFG Conf. Digest*, pp. 62–65, 2006.

[23] D. F. Williams, T. S. Clement, P. D. Hale, and A. Dienstfrey, "Terminology for high-speed sampling-oscilloscope calibration," in $68^{th}$ *ARTFG Conf. Digest*, 2006.

[24] A. V. Oppenheim and R. W. Schafer, *Digital signal processing*. Prentice Hall, 1975.

[25] M. Golio and J. Golio, *RF and Microwave Circuits, Measurements, and Modeling*. CRC, 2007.

[26] Y. Bard, *Nonlinear parameter estimation*. Academic Press, New York, 1974.

[27] W. C. Daywitt, "A simple technique for investigating defects in coaxial connectors," *IEEE Trans. Microw. Theory Tech.*, vol. 35, no. 4, pp. 460–464, 1987.

[28] "IEEE standard for precision coaxial connectors (DC to 110 GHz)," *IEEE Std 287-2007 (Revision of IEEE Std 287-1968)*, pp. C1–119, 21 2007.